Journal Pre-proofs

High throughput fabrication of zirconium titanate nanofibers by using alternating field electrospinning

Andrei Stanishevsky, Riley Yager, Sarah Nealy, Courtney Severino, Waldemar Maniukiewicz

PII: S0167-577X(22)01673-1
DOI: https://doi.org/10.1016/j.matlet.2022.133318
Reference: MLBLUE 133318

To appear in: *Materials Letters*

Received Date: 8 September 2022
Revised Date: 7 October 2022
Accepted Date: 8 October 2022

Please cite this article as: A. Stanishevsky, R. Yager, S. Nealy, C. Severino, W. Maniukiewicz, High throughput fabrication of zirconium titanate nanofibers by using alternating field electrospinning, *Materials Letters* (2022), doi: https://doi.org/10.1016/j.matlet.2022.133318

High throughput fabrication of zirconium titanate nanofibers by using alternating field electrospinning

Andrei Stanishevsky[1], Riley Yager[1], Sarah Nealy[1], Courtney Severino[1], Waldemar Maniukiewicz[2]

[1] *Department of Physics, University of Alabama at Birmingham, Birmingham, AL 35233, USA*

[2] *Faculty of Chemistry, Lodz University of Technology, 90-924 Lodz, Poland*

Abstract

Nanofibrous zirconium titanate ($Zr_{0.5}Ti_{0.5}O_2$) was derived from precursor fibers spun with a high-yield, free-surface alternating force electrospinning (AFES). A process productivity of 8.7 g/h was achived in terms of the mass of crystallized $Zr_{0.5}Ti_{0.5}O_2$ nanofibers. The average fiber diameters varied from 185 to 380 nm, depending on the annealing temperature and precursor composition. The onset crystallization temperature of the nanofibers was observed at ~640 ^{o}C irrespective to the alkoxide/polymer ratio in precursor fibers, heating rate, and fiber diameter. Nanofibrous $Zr_{0.5}Ti_{0.5}O_2$ maintained its nanocrystallinity, phase stability, and fiber integrity between 600–1200 ^{o}C. The results demonstrate strong potential of AFES for scalable production of nanofibrous zirconium titanate for demanding applications.

Keywords: Nanofibers; Zirconium Titanate; Electrospinning; Ceramics

1. Introduction

Zirconium titanate with a stoichiometric $ZrTiO_4$ (or $Zr_{0.5}Ti_{0.5}O_2$) composition is a thermally stable ternary oxide in ZrO_2–TiO_2 system [1]. It is an attractive ceramic for many applications requiring nanocrystalline materials with high surface area and porosity [2], e.g., sensors [3] and catalysts [4]. Wet chemical and sol-gel methods are the prevailing techniques to synthesize $Zr_{0.5}Ti_{0.5}O_2$ in various forms ranging from nanoparticles to macro/meso-porous monoliths [5,6]. Crystallization of $Zr_{0.5}Ti_{0.5}O_2$ from sol-gel precursors usually occurs >650 ^oC [7] but it can start at as low as 400 ^oC [8]. However, high temperature processing of nanoparticle or sol-gel based $Zr_{0.5}Ti_{0.5}O_2$ shapes reduces the porosity and surface area that can decrease the material functionality. $Zr_{0.5}Ti_{0.5}O_2$ nanofibers offer an interesting alternative because of the lack of particle aggregation, easier handling, possibility of direct three-dimensional shape formation, and improved stability. Nonetheless, there are few studies on nanofibrous $Zr_{0.5}Ti_{0.5}O_2$. For example, $Zr_{0.5}Ti_{0.5}O_2$ fibers with >600 nm diameters were prepared by drawing from a Zr and Ti salt solution [9], whereas nanofibers with 460±20 nm diameters were prepared by DC-electrospinning [3].

In this work, nanofibrous zirconium titanate was prepared by using a high-throughput alternating-field electrospinning (AFES, a.k.a. AC-electrospinning) technique, demonstrated earlier for TiO_2 and ZrO_2 nanofiber fabrication [10,11]. AFES generates dense, slowly propagating fibrous flows, which allows easy collection and handling of as-spun fibers. This study is an initial assessment of AFES for sizeable production of zirconium titanate nanofibers. The main goals were to examine the process performance and effects of the annealing temperature and precursor composition on crystallization of stoichiometric $Zr_{0.5}Ti_{0.5}O_2$ nanofibers.

2. Materials and Methods

2.1. Precursor preparation

A 0.5:0.5:0.8:0.2 molar mixture of titanium n-Butoxide ($Ti(OBu)_4$), zirconium propoxide ($Zr(OPr)_4$, 70 wt% in 1-propanol), glacial acetic acid and acetylacetone (Alfa Aesar) was prepared in ethanol (200 Proof, Decon Labs) and added to an ethanol solution of polyvinylpyrrolidone (PVP, M_w=1,300,000) with hydroxypropyl cellulose (HPC, M_w=100,000) (Scientific Polymer Products). The PVP/HPC mass ratio was 1:1, and the alkoxide/polymer mass ratio was set to yield 1.0, 1.5, and 2.0 grams of $Zr_{0.5}Ti_{0.5}O_2$ per one gram of polymer. The precursors and resulting nanofibers were labeled as ×1.0, ×1.5, and ×2.0, respectively. The polymer concentration was 5 wt% in each precursor.

2.2. Fabrication of nanofibers

The precursor solution was supplied by a syringe pump to a dish-shaped, 25 mm diameter AFES electrode operated at 25–33 kV rms AC voltage [10,11]. The generated precursor fibers were deposited on a PTFE mesh placed ~50 cm above the electrode. The collected fibrous bulk was heated at 2 ^{o}C/min and calcined at 600–1200 ^{o}C for 3 hours in air in a programmable furnace (Isotemp, Fisher Scientific).

2.3. Characterization

Thermogravimetric Analysis (TGA, SETARAM, France) was performed in air at 10 ^{o}C/min heating rate. Thermogravimetric (TG), differential thermal analysis (DTA), differential thermogravimetric (DTG), and ion emission signals were recorded simultaneously. ASAP2020 adsorption analyzer (Micromeritics) was used to determine the fiber surface area and pore parameters. The surface morphology and elemental composition of nanofibers were analyzed by using FEI Quanta 650 SEM equipped with an EDS detector. EDS data were averaged over ten

100×100 μm^2 areas. Fiber diameters were determined by ImageJ. X-ray diffraction (XRD) patterns were recorded at room temperature and during the heating at 2 and 20 ^{o}C/min by using a PANalytical X'Pert Pro MPD diffractometer equipped with a 900 ^{o}C hot stage. PANalytical High Score Plus software package and ICDD powder diffraction file (PDF-2 ver.2013) database were used for data analysis.

3. Results and Discussion

AFES with all tested precursors produced a uniform fibrous flow, which propagated at 0.8–0.9 m/s with little fiber bundling at 29±2kV rms AC voltage (Fig.1a). AC voltages below and above that range produced less stable flows. The precursor flow take-off rate varied from 80 to 93 mL/h with the increasing concentration of alkoxide in the precursor (Fig.1b). The quantities of the collected fibrous bulk corresponded to the production rate of 3.6–8.7 g/h in terms of $Zr_{0.5}Ti_{0.5}O_2$ mass. The volume of as-spun material produced from ~20 mL of ×1.5 precursor solution is shown in inset in Fig.1a. All fibers, irrespective of the precursor composition, had smooth surface morphology after the annealing at 600 ^{o}C, which was retained after the annealing at up to 800 ^{o}C (Fig.1c). At this stage, surface voids with up to 35 nm diameters are seen, especially in ×1.0 nanofibers (Fig.1c, insets). The fiber diameters (Table 1 and Fig.1d) show little change after the annealing at 800 and 1000 ^{o}C except ×1.0 fibers, which is related to their larger radial shrinkage because of initially higher meso-porosity (Table1). The increase of fiber diameters in all samples at higher annealing temperatures is explained by axial fiber shrinkage due to the crystallites coalescence, grains growth and change of their shape, and destruction of a fraction of nanofibers with smaller diameters. The N_2 adsorption/desorption analysis was unreliable for those samples.

TGA and XRD analyses revealed the same trends in all tested fibers. TG data show ~45, 52, and 56% of initial mass remained in of ×1.0, ×1.5, and ×2.0 fibers, respectively, after the annealing at <520 °C (Fig.2a,b). The mass change was negligible between 520 and 660 °C, although the ion emission signals showed the continuing removal of residual carbon. Additional ~2% mass loss was observed between 660–700 °C due to the removal of the remaining carbon. An exothermic peak at ~680 °C is due to fast crystallization of the fibers. XRD data show that all nanofibers remain amorphous up to 640 °C, when the initial crystallization of $Zr_{0.5}Ti_{0.5}O_2$ (ICDD PDF #01-074-9432) starts (Fig. 2c-e) irrespective to the as-spun fiber composition, heating rate, fiber diameter and porosity. Nearly full crystallization occurs at 690±10 °C. However, even ~1 mol% excess Zr (Fig.2c) triggered the crystallization of $Zr_{0.5}Ti_{0.5}O_2$ at 600 °C. XRD peaks from a minor, monoclinic *m*-ZrO_2 phase become well-defined in 1200 °C annealed material. The excess Ti (up to 5 mol%) did not reveal the formation of other crystalline phases. The heating rate (Fig.2f) and initial fiber composition had little effect on the crystallite sizes and their change with the increasing temperature. The crystallite sizes remain within 20–25 nm after the annealing at 1000 °C, and they increase to 30–45 nm after the annealing at 1200 °C.

Detailed SEM analysis of $Zr_{0.5}Ti_{0.5}O_2$ nanofibers show the apparently grainy, nanoparticle-like inner microstructure of 600 °C fibers (Fig.3a,b), regardless the initial fiber composition, although those fibers are X-ray amorphous. Fully crystallized nanofibers show similar grainy structure after the annealing at 800 °C (Fig.3c,d). Thus, the annealing of as-spun fibers leads, perhaps, to initially clustered, amorphous $Zr_{0.5}Ti_{0.5}O_2$ nanoparticle structure with 20–30 nm particle size. The temperature >640 °C triggers the nucleation of $Zr_{0.5}Ti_{0.5}O_2$ crystallites inside the particles. Further crystallization and development of $Zr_{0.5}Ti_{0.5}O_2$ nanofiber microarchitecture and surface morphology is determined by the competition between the crystallite and particle growth

and coalescence within a porous fiber framework. The fiber diameter noticeably affects the fiber shape and interfiber fusion due to partial sintering when annealed at 1000 and 1200 °C (Fig.3e-h). Some smaller diameter fibers break down at 1200 °C (Fig.3g) but the overall mechanical integrity of nanofibrous $Zr_{0.5}Ti_{0.5}O_2$ material is maintained.

4. Conclusions

High-throughut AC-electrospinning has been used for the first time for sizeable production of nanofibrous stoichiometric zirconium titanate. In the used experimenal setup, up to 8.7 g/h productivity was achieved in terms of the mass of crystallized $Zr_{0.5}Ti_{0.5}O_2$. The crystallization of stoichiometric $Zr_{0.5}Ti_{0.5}O_2$ nanofibers starts at ~640 °C from a clusterized, amorphous nanoparticle-like structure, and the material becomes fully crystallized at ~690 °C regardless the initial alkoxide/polymer ratio, fibers diameter and their heating rate. For all tested precursor compositions, the nanofibrous $Zr_{0.5}Ti_{0.5}O_2$ reveals the 12–45 nm crystallite size and phase stability after thermal processing in the temperature range of 600–1200 °C.

CRediT authorship contribution statement

Andrei Stanishevsky: Conceptualization, Data curation, Writing - original draft. Riley Yager: Investigation, Validation, Writing – review & editing. Sarah Nealy: Methodology, Investigation, Courtney Severino: Methodology, Investigation. Waldemar Maniukiewicz: Investigation, Formal analysis.

Conflicts of interest

The authors declare that they have no known competing financial interests or personal relationships that could influence the work reported in this paper.

Acknowledgements

This work was supported by the National Science Foundation (NSF, Grant #1708600). R.Y., S.N., and C.S. acknowledge the support from NSF International Research Experience for Students Program (Grants #1558268 and #1852207).

References

1. U. Troitzsch, D.J. Ellis, The ZrO_2-TiO_2 phase diagram, J. Mater. Sci. 40 (2005) 4571-4577.
2. J. Macan, A. Gajović, H. Ivanković, Porous zirconium titanate ceramics synthesized by sol-gel process, J. Eur. Ceram. Soc. 29 (2009) 691-696.
3. I.C. Cosentino, E.N.S. Muccillo, R. Muccillo, Development of zirconia–titania porous ceramics for humidity sensors. *Sens. Actuators B* 96 (2003) 677–683.
4. A.S. Yasin, M. Obaid, M.H. El-Newehy, S.S. Al-Deyab, N.A.M Barakat, Influence of $Ti_xZr_{(1-x)}O_2$ nanofibers composition on the photocatalytic activity toward organic pollutants degradation and water splitting, Ceram. Int. 41 (2015) 11876–11885.
5. F. Khairulla, P.P. Phule, Chemical synthesis and structural evolution of zirconium titanate, Mater. Sci. Eng. B, 12 (1992) 327-336.
6. M. Sun, T. Zhao, Z. Ma, Z. Li, Facile preparation of macro-mesoporous zirconium titanate monoliths via a sol-gel reaction accompanied by phase separation, J. Mater. Res. 34 (2019) 4066-4075.

7. L.M. Oanh, D.B. Do, N.M. Hung, D.V. Thang, D.T. Phuong, D.T. Ha, N. Van Minh, Formation of Crystal Structure of Zirconium Titanate $ZrTiO_4$ Powders Prepared by Sol–Gel Method, J. Electronic Mater. 45 (2016) 2553-2558.
8. I.C. Cosentino, E.N.S. Muccillo, R. Muccillo, F.M. Vichi, Low-temperature sol-gel synthesis of single-phase $ZrTiO_4$ nanoparticles, J. Sol-Gel Sci. Technol. 37 (2006) 31-37.
9. Q. Lu, D. Chen, X. Jiao, Synthesis of long $ZrTiO_4$ fibers by a sol-gel process free of organic components, J. Mater. Chem. 13 (2003) 1127-1131.
10. A. Stanishevsky, R. Yager, J. Tomaszewska, M. Binczarski, W. Maniukiewicz, I. Witońska, D. Lukas, Structure and mechanical properties of nanofibrous ZrO_2 derived from alternating field electrospun precursors, Ceram. Int. 45 (2019) 18672.
11. S. Nealy, C. Severino, A. Brayer, A. Stanishevsky Nanofibrous TiO_2 produced using alternating field electrospinning of titanium alkoxide precursors: crystallization and phase development, RSC Adv. 10 (2020) 6840-6849.

Table 1. Diameters and textural properties of $Zr_{0.5}Ti_{0.5}O_2$ nanofibers annealed at 600 and 800 °C.

Sample	Average diameter, nm	BET surface area, m^2/g	Total pore volume, cm^3/g	Mean pore diameter, nm
×1.0	208/189	58.0/31.6	0.31/0.21	19.2/26.0
×1.5	263/259	44.3/22.4	0.25/0.13	22.5/25.3
×2.0	370/365	41.4/24.1	0.23/0.14	22.3/23.7

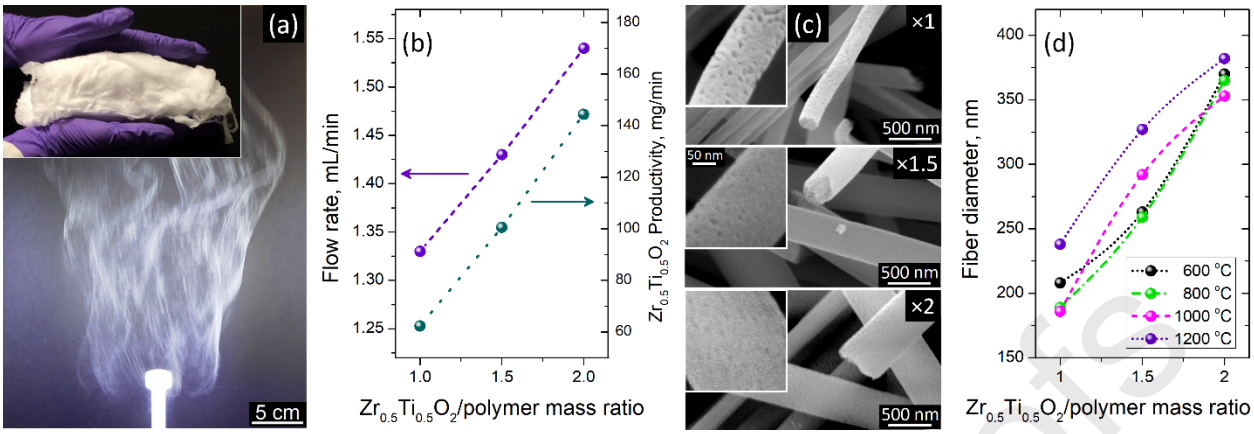

Fig.1. (a) Representative AFES generated fibrous flow and as-spun material. (b) Precursor flow take-off rate and process productivity in terms of $Zr_{0.5}Ti_{0.5}O_2$ nanofiber mass, (c) Fiber surface morphology after the annealing at 800 °C, and (d) fiber diameter after the annealing at different temperatures *vs* alkoxide/polymer mass ratio in the precursor solution.

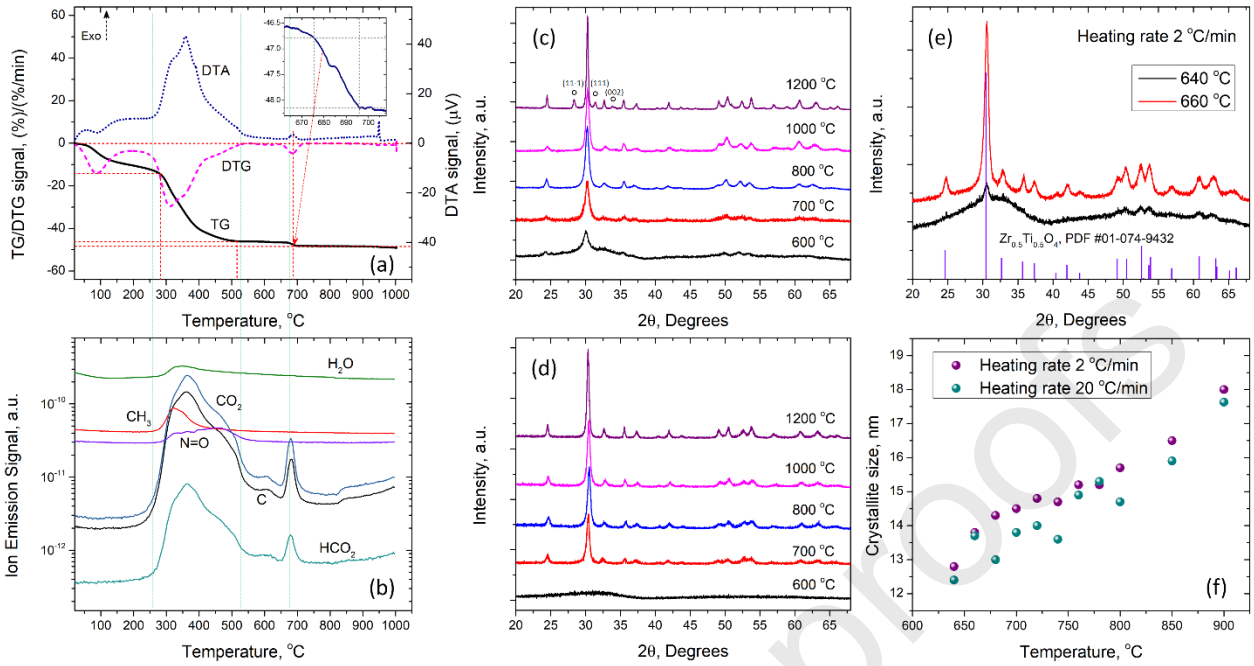

Fig.2. (a) TGA and (b) ion emission signals of ×1.5 as-spun fibers, (c,d) XRD patterns of (c) Zr-rich (open circles denote *m*-ZrO_2 peaks) and (d) stoichiometric $Zr_{0.5}Ti_{0.5}O_2$ ×1.5 nanofibers annealed at different temperatures, (e,f) effect of heating rate on fiber crystallization and crystallite size.

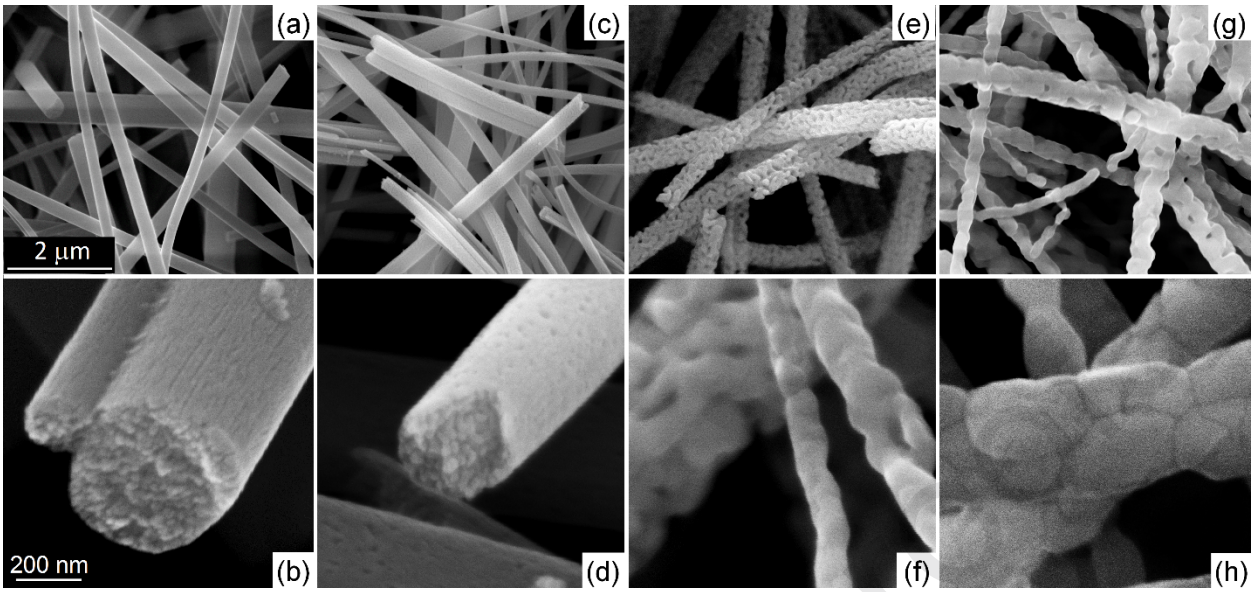

Fig.3. SEM images of $Zr_{0.5}Ti_{0.5}O_2$ nanofibers prepared from ×1.5 precursor solution and annealed at (a,b) 600, (c,d) 800, (e,f) 1000 and (g,h) 1200 ºC.